Applied Catalysis A, General 545 (2017) 79–89

Contents lists available at ScienceDirect

Applied Catalysis A, General

journal homepage: www.elsevier.com/locate/apcata

Feature Article

Conversion of propionic acid and 3-pentanone to hydrocarbons on ZSM-5 catalysts: Reaction pathway and active site

Xuefen Wang[a], Shuang Ding[a], Hua Wang[a], Xiao Liu[a], Jinyu Han[a], Qingfeng Ge[a,b,**], Xinli Zhu[a,*]

[a] Collaborative Innovation Center of Chemical Science and Engineering, School of Chemical Engineering and Technology, Tianjin University, Tianjin 300072, China
[b] Department of Chemistry and Biochemistry, Southern Illinois University, Carbondale, IL 62901, United States

ARTICLE INFO

Keywords:
Propionic acid
3-Pentanone
Ketonization
Aldol condensation
Reaction pathway

ABSTRACT

Conversion of propionic acid to gasoline-range molecules was investigated at 350 °C on a series of ZSM-5 catalysts with varying density of Brønsted acid sites (BAS), achieved by ion exchange of proton with Na^+. Ketonization of propionic acid to 3-pentanone is the primary reaction, with the sequential aldol condensation to dipentanone alcohol being the secondary. The major reaction pathway for forming the aromatics involves dehydration, cyclization, dehydration and hydride transfer from dipentanone alcohol, leading to the formation of C_{10} aromatics before being dealkylated to lighter aromatics. Temperature programmed desorption of propionic acid indicates that the reaction initiates with acylium cation formation on BAS through dehydration. Comparing the turnover frequencies of ketonization and aldol condensation on ZSM-5 with varying density of BAS indicates that BAS is the active site for both reactions. The propionic acid feed deactivates the catalyst faster than the 3-pentantone feed due to a stronger adsorption of propionic acid on the acid sites of ZSM-5.

1. Introduction

Energy derived from biomass is considered renewable and environmentally friendly and has attracted increasing attentions [1,2]. Fast pyrolysis breaks the lignocellulosic biomass into oxygenated bio-oil, including compounds such as aldehydes, ketones, carboxylic acids, alcohols, furanics, phenolics, and so on [3,4]. Upgrading bio-oil to reduce the oxygen contents is necessary to improve its heating value and stability as well as reduce its corrosiveness and viscosity. Short chain carboxylic acids are a main fraction of bio-oil, and are the main contributor to the corrosiveness of the bio-oil. Upgrading carboxylic acids to stable and non-corrosive products that are compatible with gasoline and diesel is of great importance.

Recently, ketonization of carboxylic acids on metal oxides catalysts have been extensively studied [5–7]. On the other hand, zeolite catalyzed oxygenates to hydrocarbons have been studied since the discovery of methanol conversion to gasoline on HZSM-5 [8,9], and have been applied to upgrading bio-oil and its model compounds [10–14]. However, relatively fewer studies have been performed on conversion of carboxylic acids on zeolite, possibly due to the fast deactivation of catalyst and complex products distribution. Previous brief study of acetic acid conversion on acidic zeolite suggested that acetone is the primary product, with olefins, paraffins and aromatics being the secondary products [15,16]. These authors also suggested that ketonization of acetic acid involves the surface acetyl by dehydration and a nucleophilic attack, resulting in CO_2 elimination and acetone formation [2,17–20]. Studies of acetone conversion on zeolite indicated that the aldol condensation to dimer and trimer is the primary reaction, which can then be converted to aromatics and other products through a series of complex secondary reactions [21–23].

ZSM-5 is a three-dimensional zeolite, which contains well-defined and interconnected zigzag (0.53 nm × 0.56 nm) and straight (0.51 nm × 0.55 nm) channels. Bridging hydroxyl in HZSM-5 serves as Brønsted acid sites, which enables the acid-catalyzed reactions with shape selectivity. Thus, ZSM-5 has been widely used in many industrial processes.

Little work has been reported on the conversion of propionic acid on HZSM-5 in the literature. In this work, propionic acid was selected as a model compound to study the reaction pathway of carboxylic acids conversion on HZSM-5, with 3-pentanone studied for comparison. Propionic acid could also be a simple model compound of carboxylic acid derived from bio-diesel and used to study bio-diesel conversion on zeolite. Through Na ion-exchange, a series of HNaZSM-5 with varying density of Brønsted acid sites was prepared and tested for propionic acid conversion. The results indicated that Brønsted acid sites are the active sites for both ketonization of propionic acid and sequential aldol

---

[*] Corresponding author.
[**] Corresponding author at: Department of Chemistry and Biochemistry, Southern Illinois University, Carbondale, IL 62901, United States.
E-mail addresses: qge@chem.siu.edu (Q. Ge), xinlizhu@tju.edu.cn (X. Zhu).

http://dx.doi.org/10.1016/j.apcata.2017.07.037
Received 19 April 2017; Received in revised form 20 July 2017; Accepted 24 July 2017
Available online 26 July 2017
0926-860X/ © 2017 Elsevier B.V. All rights reserved.

condensation.

2. Experimental

2.1. Catalyst preparation

The HZSM-5 catalyst (denoted as HZ) was obtained by calcination of NH_4ZSM-5 (Zeolyst, CBV 8014, Si/Al = 40, $S_{BET} = 425\ m^2/g$) at 550 °C for 8 h. Ion exchange of NH_4ZSM-5 (2 g) with different concentrations (0.01, 0.1, 0.5 and 1 M) of $NaNO_3$ solution (100 mL) was carried out at 80 °C for 5 h. The resulting material was filtered, washed with de-ionized water, and dried overnight at 100 °C. The ion-exchange procedure was performed once in 0.01, 0.1, 0.5 M $NaNO_3$ solution, while it was repeated 4 times in 1 M $NaNO_3$ solution to maximize the degree of exchange. Finally, these samples were calcined at 550 °C for 8 h to obtain the HNaZSM-5 catalysts, which were denoted as HNaZ-1, HNaZ-2, HNaZ-3 and HNaZ-4, respectively, corresponding to $NaNO_3$ concentrations of 0.01, 0.1, 0.5 and 1 M, respectively. The resulting catalyst powder was pressed, crushed, and sieved to 40–60 mesh for catalytic evaluation.

2.2. Catalyst characterization

Elemental analysis was done on a VISTA-MPX inductively coupled plasma-optical emission spectrometer (ICP-OES). The samples were dissolved in HF solution and diluted before measurements. The powder X-ray diffraction (XRD) patterns were measured on a Rigaku D/max 2500 diffractometer, with a Cu Kα radiation (40 kV, 200 mA) source. Data was collected in 2θ range of $4-60°$ at a scanning rate of 4°/min. The scanning electron microscopy (SEM) images of gold-coated samples were recorded on a FEI NANOSEM430 instrument. N_2 adsorption was carried out on a Tristar 3000 analyzer (Micromeritics) at liquid nitrogen temperature. Prior to the experiments, samples were outgassed at 300 °C for 3 h.

The diffuse reflectance infrared Fourier transform spectroscopy (DRIFTS) was conducted on a PerkinElmer Frontier spectrometer, equipped with a liquid nitrogen cooled mercury cadmium telluride (MCT) detector, a diffuse reflectance accessory and a reaction chamber (Harrick). The catalyst powder was pretreated in flowing He (30 mL/min) stream at 450 °C for 1 h. Following that, the sample was cooled to 20 °C, and the DRIFTS was recorded with 128 scans at a resolution of 2 cm^{-1}. The spectrum of KBr powder was used as a reference. For the experiments of pyridine adsorption, the sample after pretreatment was cooled to 100 °C, and a background spectrum was recorded. The pyridine vapor was introduced for 10 min and the sample was held at this temperature for another 20 min. Then the temperature was increased to 150 °C and maintained for 30 min. The DRIFTS spectra of pyridine adsorption were then recorded with 32 scans at a resolution of 8 cm^{-1}.

Temperature programmed desorption of NH_3 (NH_3-TPD) and isopropylamine (IPA-TPD) were performed in a quartz tube reactor (o.d. = 6 mm), equipped with temperature controller and gas delivery system, as has been reported in previous work [24]. The catalyst sample of 50 mg (40–60 mesh) were pretreated in flowing He (30 mL/min) at 400 °C for 1 h and then cooled to 100 °C. The sample was then exposed to NH_3 (2% NH_3/He, 30 mL/min) for 30 min or to IPA (2 μL/pulse, pulse/3 min, 10 pulses). After that, the sample was flushed with He flow for 1 h to remove weakly adsorbed NH_3 or IPA, followed by heating up to 650 °C at a rate of 10 °C/min. The effluent was monitored by a Cirrus 200 mass spectrometer (MKS). Temperature Programmed Oxidation (TPO) of spent catalyst sample was performed in the same system. In this case, the sample (50 mg) was heated from 30 to 900 °C in flowing 5% O_2/He (30 mL/min) with a linear heating rate of 10 °C/min. Quantification was carried out by injecting 250 μL of NH_3, propylene, CO_2 and CO pulses to the He stream using a six-port valve.

2.3. Catalytic activity

The catalytic conversions of propionic acid and 3-pentanone were investigated in a fixed-bed quartz tube (o.d. = 6 mm) reactor. The catalyst sample (40–60 mesh) was packed in the middle of the reactor and pretreated in flowing Ar at 350 °C for 0.5 h before adjusted to the reaction temperature. Liquid reactant was fed from a 5 mL Hamilton syringe using a KDS-100 syringe pump (KD Scientific), and was vaporized before entering the reactor. Argon was used as the carrier gas with a Feed/Ar molar ratio of 1/25. The space time (W/F, defined as weight of catalyst (g) to the flow rate of the organic feed (g/h)) was adjusted from 0.02 to 3.5 $g_{cat}{\cdot}h/g_{reactant}$ (h) to monitor the major products evolution. The stream after reaction was maintained at 220 °C to avoid any condensation and sampled frequently through a six-port valve to an *online* gas chromatograph (GC 7890B, Agilent) for products quantification. The GC was equipped with an HP-Innowax column (60 m × 320 μm × 0.5 μm) and a flame ionic detector. N_2 was used as carrier gas for GC, and a column flow rate of 1.8 mL/min with a split ratio of 20 was used. The column was heated from 40 to 240 °C in several steps with different heating rates to achieve good separation of products. The reaction effluents were finally trapped in a methanol solvent at 0 °C in an ice-water bath. The resulting solution was injected to an offline gas chromatography-mass spectrometer (GC–MS, Shimadzu QP2010SE) for products qualification. The GC–MS was also equipped with an HP-Innowax column (30 m × 320 μm × 0.5 μm), and operated under a similar condition to that of online GC. The conversion (%) is defined as 100% × [(moles of carbon of reactant in the feed) − (moles of carbon of reactant in the effluent)]/(moles of carbon of reactant in the feed). Because CO_2 cannot be monitored by FID, and taking into account the reaction stoichiometry of ketonization, the yield (%) is defined as 100% × [6 × (moles of carbon of product in the effluent)]/[5 × (moles of carbon of reactant in the feed)] for the propionic acid feed. For the 3-pentanone feed, the yield (%) is defined as 100% × (moles of carbon of product in the effluent)/(moles of carbon of reactant in the feed). The selectivity (%) is defined as 100% × yield/conversion. The uncertainties from multiple runs were within ± 2%. CO_2 produced in the reaction was quantified for selected runs using another 7890B GC, equipped with a thermal conductive detector and a Porapak Q column. The carbon balance was estimated to be higher than 95%.

Temperature-programmed reaction of propionic acid over HZ and HNaZ-4 were studied in the TPD system, as described in previous section. Catalyst sample of 50 mg (40–60 mesh) was pretreated in a flowing He stream (30 mL/min) at 400 °C for 1 h before the temperature was reduced to 100 °C and propionic acid of 1 μL was injected manually. The injection was repeated 16 times every 3 min to ensure the saturated adsorption of propionic acid on the catalyst surface. The sample was then flushed by flowing He (70 mL/min) for 1 h to remove weakly adsorbed propionic acid. After that, the He flow rate was reduced to 30 mL/min, and the sample was kept at 100 °C for an additional 15 min to ensure the MS signals returned to the base line. Finally, the sample was heated to 600 °C at a heating rate of 10 °C/min.

3. Results and discussion

3.1. Catalysts characterization

Table 1 summarizes the chemical analysis results from ICP. The Si/Al ratio is similar to the manufacture provided value of 40, and changes slightly after Na exchange. The Na/Al ratio increases with the increasing Na concentration as well as exchange cycles, indicating that Na was successfully loaded onto the zeolites. Fig. 1 compares the XRD patterns of HZ and HNaZ-4 samples. Although the peak intensity was slightly reduced for HNaZ-4, it is evident that the MFI structure of ZSM-5 zeolite was well preserved after ion exchange. The morphology of the zeolite was shown in SEM images. The HZ particles have irregular shape

Table 1
Si/Al ratio, Na/Al ratio, surface area (S_{BET}), total acid density (A_{total}) and Brønsted acid density (A_{BAS}) of ZSM-5 catalysts.

Sample	Si/Al[a]	Na/Al[a]	S_{BET} (m^2/g)	A_{total}[b] (μmol/g)	A_{BAS}[c] (μmol/g)
HZ	37.5	0.04	379	880	384
HNaZ-1	35.7	0.35	n.d.[d]	780	248
HNaZ-2	37.3	0.63	n.d.[d]	800	172
HNaZ-3	36.0	0.78	n.d.[d]	812	113
HNaZ-4	39.2	0.89	364	995	43

[a] measured by ICP.
[b] measured by NH_3-TPD.
[c] measured by IPA-TPD, calibrated by NH_3.
[d] not determined.

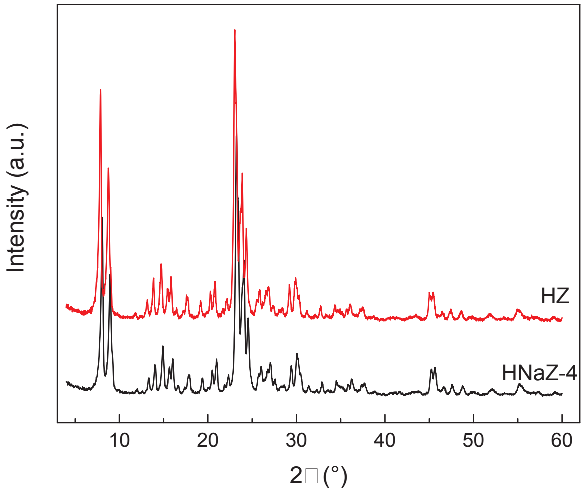

Fig. 1. XRD patterns of HZ and HNaZ-4.

with sizes in the range of 0.2–1.0 μm (Fig. 2A). The ion exchanged HNaZ-4 (Fig. 2B) has similar morphology and size to those of HZ, indicating that ion-exchange does not affect the particle morphology and sizes. The BET specific surface areas were similar for the HZ and HNaZ-4 samples (Table 1), indicating that Na exchange has little effect on the pore structure. In summary, these results demonstrated that the Na exchange procedure caused neither damage to the framework structure nor changes to the morphology and surface areas. This is expected since the exchange was performed in a neutral pH solution, and the high Si/Al ratio of zeolite resulted in a low amount of Na being exchanged onto the zeolite.

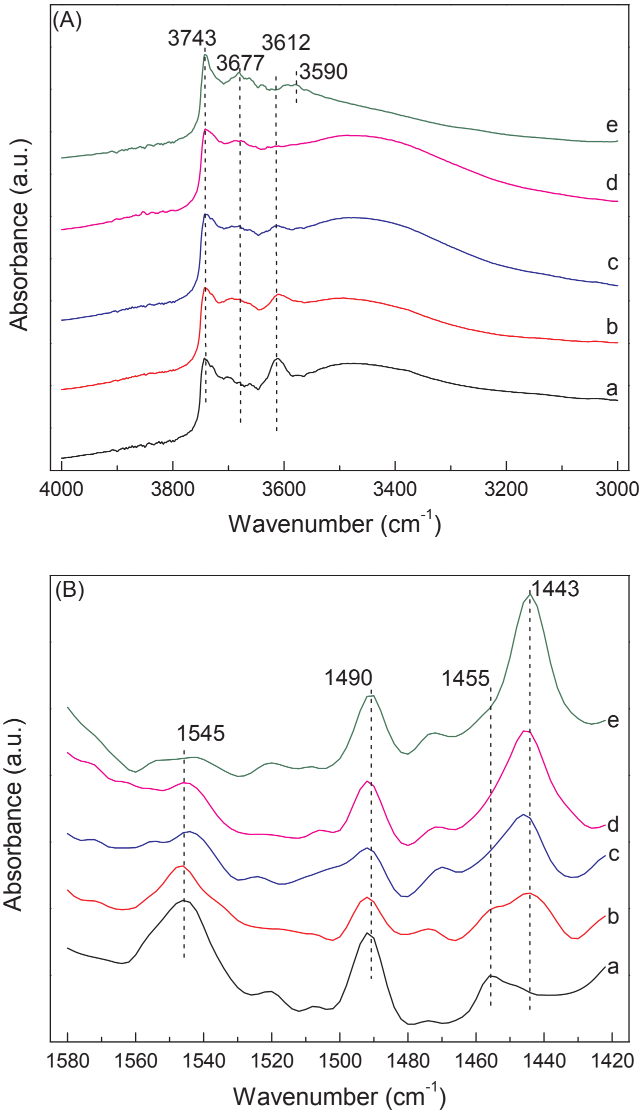

Fig. 3. DRIFTS of (A) hydroxyl stretching region and (B) pyridine adsorption of (a) HZ, (b) HNaZ-1, (c) HNaZ-2, (d) HNaZ-3, and (e) HNaZ-4.

The structural evolution as a function of increasing degree of Na exchange was followed by DRIFTS of the hydroxyl stretching region. As shown in Fig. 3A, two bands at 3743 and 3612 cm^{-1} are present in the HZ sample, which can be assigned to terminal Si-OH and bridging Si-OH-Al (Brønsted acid site, BAS), respectively [25–29]. As the degree of exchange increases, the band at 3612 cm^{-1} decreases and eventually disappeared, confirming the replacement of proton by Na^+. Concurrently, a weak band at 3677 cm^{-1} develops in the HNaZ samples and becomes significant in HNaZ-4, accompanied by a weak band at

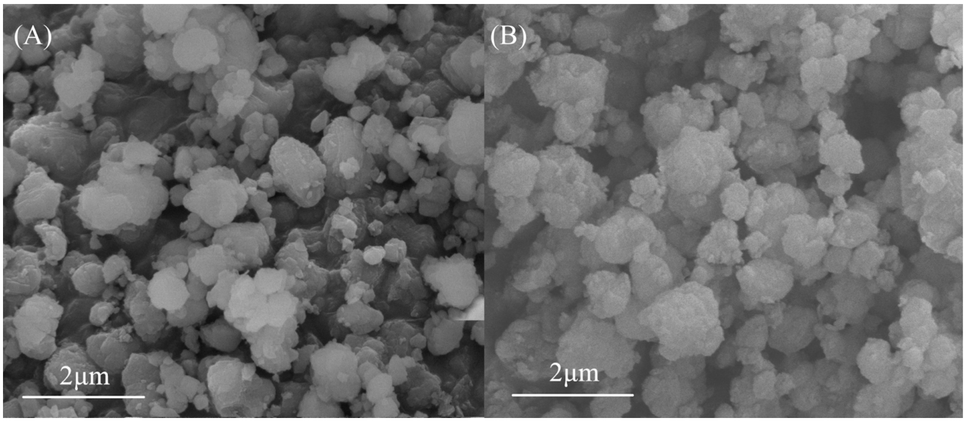

Fig. 2. SEM images of (A) HZ and (B) HNaZ-4.

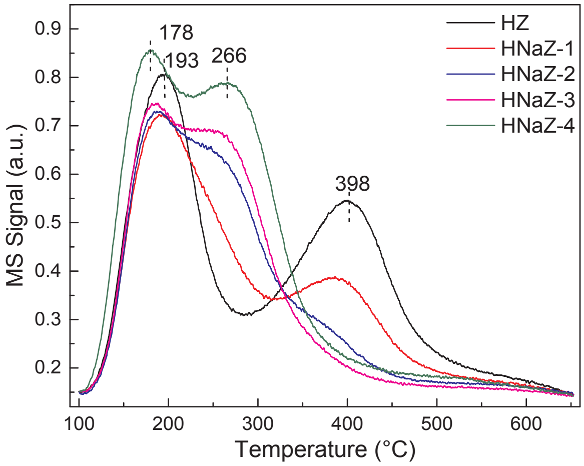

Fig. 4. NH_3-TPD profiles of the HZSM-5 (HZ) and HNaZSM-5 samples (HNaZ-1 to HNaZ-4).

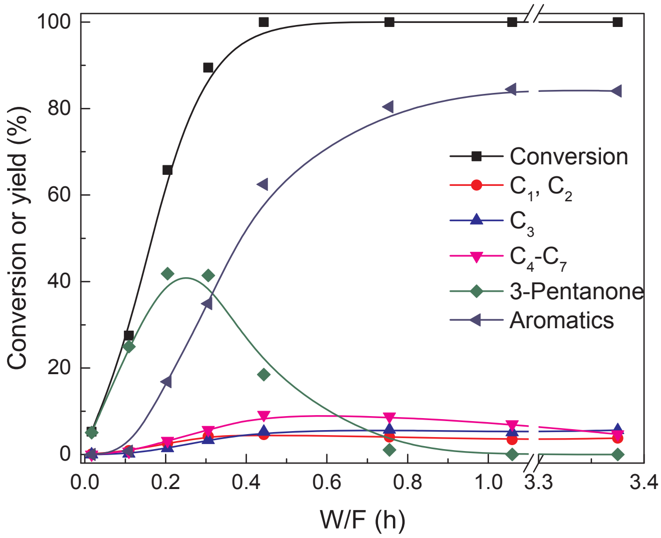

Fig. 6. Propionic acid conversion and products distribution as a function of space time (W/F) on HZ. Reaction conditions: T = 350 °C, P = 1 atm, Time on stream is 0.5 h for each W/F.

3590 cm^{-1}. These bands are associated with Al-OH of extra and/or partial framework alumina species [27], suggesting dealumination may have taken place during the ion exchange, particularly for HNaZ-4. The little change of Si/Al ratio (Table 1) may imply that dealumination is not severe, with few Al ions being leached away from the zeolite. In addition, the broad band centered at ~3400 cm^{-1} observed in other samples was significantly reduced for this sample. As this band was believed to relate to the hydrogen bonded hydroxyls, its reduction suggests that excess Na^+ may be exchanged to the silanol nests [29].

The acidity of the samples was investigated using DRIFTS measurement of pyridine adsorption, NH_3-TPD and IPA-TPD. As displayed in Fig. 3B, the band at 1545 cm^{-1} is attributed to protonated pyridine on BAS, while the band at 1455 cm^{-1} is related to the coordinative adsorption of pyridine on the Lewis acid site (LAS) of Al cations [30]. Apparently, the HZ sample contains mainly BAS. As the degree of exchange increases, the intensity of the BAS band decreases. In the meantime, the band of LAS shifts to 1443 cm^{-1} and increases in intensity. This latter band is assigned to pyridine adsorption on LAS of Na^+, which has a weak acidity [31]. The results show that the replacement of proton with Na^+ leads to weak LAS. The presence of the 1545 cm^{-1} band for HNaZ-4 indicates that the protons have not been completely replaced even after several exchange cycles. It should be noted that intensity of the band at 1455 cm^{-1} was little changed, confirming the low degree of dealumination upon ion exchange.

As shown in Fig. 4, two peaks at 193 and 398 °C were observed in the NH_3-TPD profile of HZ sample, which are usually assigned to weak acid sites and strong acid sites (most probably to be BAS), respectively [32–36]. As Na increases in the exchanged samples, the peak associated with the strong acid sites reduces and shifts to a lower temperature. Meanwhile, a new peak at 266 °C starts to develop. This new peak is believed to originate from desorption of NH_3 on the weak LAS of Na^+ cations [31,37,38], which is consistent with the DRIFTS of pyridine adsorption.

Fig. 5 compares the IPA-TPD profiles of different samples. According to Hofmann elimination reaction, IPA undergoes decomposition to propene and ammonia on BAS but not on LAS [39], which is routinely used to quantify the acid density of BAS [40]. The resulting propene ($m/z = 41$) and NH_3 ($m/z = 16$) on BAS were observed at 353 and 378 °C, respectively. The molecularly adsorbed IPA ($m/z = 44$) at the weak acid sites of Si-OH was observed at 203 °C for HZ [10,41]. As the degree of exchange increases, the intensity of the propene and NH_3 peaks decreases. A weak peak at 421 °C was observed for highly exchanged sample. This week peak may be assigned to adsorption on BAS of weaker acidity, such as Al-OH of partial framework alumina. Interestingly, the peak intensity associated with Si-OH at 203 °C decreases (Fig. 5A) with increasing degree of exchange, accompanied by a new

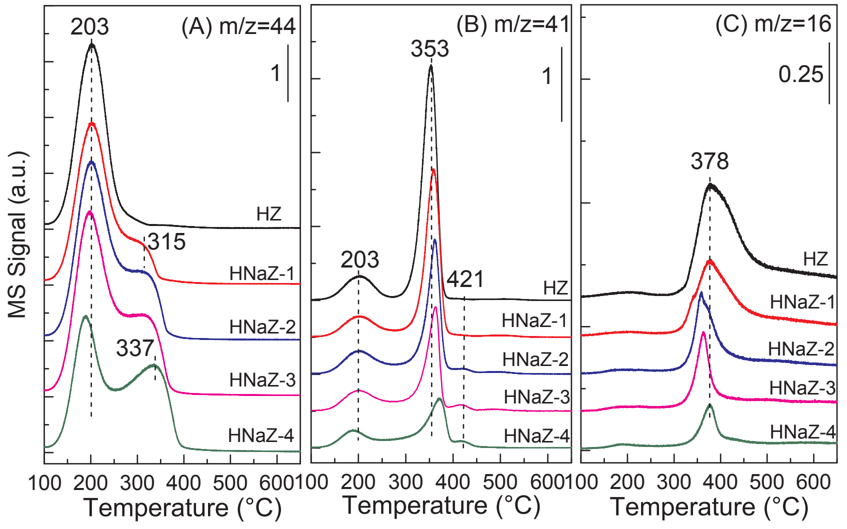

Fig. 5. IPA-TPD profiles of (A) $m/z = 44$, (B) $m/z = 41$, and (C) $m/z = 16$ of HZSM-5 (HZ) and HNaZSM-5 samples (HNaZ-1 to HNaZ-4).

Table 2
Products distribution during propionic acid conversion on HZ.[a]

W/F (h)	0.02	0.11	0.20	0.31	0.44	3.37
Conversion (%)	5.1	27.5	65.8	89.5	100	100
Yield of major products (%)						
3-Pentanone	5.1	25.0	41.8	41.4	18.5	0
C_1-C_2	0	0.89	2.6	4.2	4.6	3.8
C_3	0	0.18	1.4	3.3	5.3	5.6
C_4-C_7	0	0.69	3.1	5.7	9.2	4.7
Benzene	0	0	0.14	0.4	0.7	2.7
Toluene	0	0	0.65	1.9	4.3	12.0
C_8 aromatics						
Ethylbenzene	0	0	0.59	1.5	2.4	1.9
p-Xylene	0	0	0.9	2.8	5.0	4.3
m-Xylene	0	0	1.7	3.2	6.3	9.4
o-Xylene	0	0	0.63	1.8	2.8	4.2
C_9 aromatics						
Methylethylbenzene	0	0	1.2	2.3	5.9	3.1
1,2,4-Trimethylbenzene	0	0	0.54	1.5	3.4	4.5
C_{10+} aromatics						
1,3-Dimethyl-4-ethylbenzene	0	0.15	1.1	2.0	2.8	0.6
5-Methylindane	0	0	0.57	1.2	1.9	1.3
1-Methylnaphthalene	0	0	0.48	1.1	2.7	8.8
1,7-Dimethylnaphthalene	0	0.23	1.2	2.8	5.7	8.9
Other C_{10+}[b]	0	0.36	7.2	12.4	18.5	24.2

[a] Reaction conditions: T = 350 °C, P = 1 atm, Time on stream is 0.5 h for each W/F.

[b] other C_{10+} aromatics include: 1-allyl-2-methylbenzene, 1-methyl-2-propylbenzene, 1-methyl-3-propylbenzene, 1-methyl-4-propylbenzene, 1,4-diethylbenzene, 1,2-diethylbenzene, 4,7-dimethylindene, 2-methyl-1,2-dihydronaphthalene, 7-methyl-1,2-dihydronaphthalene, 1,3-dimethylindene, 4,7-dimethylindane, 5,6-dimethylindane, 1,2-dimethylindane, 7-ethyl-1,2-dihydronaphthalene, 1,4,6-trimethylnaphthalene, 1,4,5-trimethylnaphthalene.

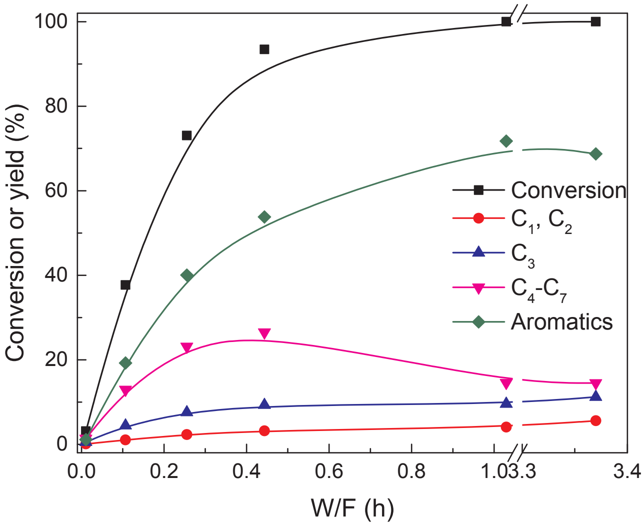

Fig. 8. 3-Pentanone conversion and major products distribution as a function of W/F on HZ. Reaction conditions: T = 350 °C, P = 1 atm, Time on stream is 0.5 h for each W/F.

Table 3
Product distribution during reaction of propionic acid and 3-pentanone mixture on HZ.[a]

Propionic acid content in feed (%)	Propionic acid content in products (%)	3-Pentanone content in products (%)	Others content in products (%)
100	89.8	9.7	0.52
82	71.3	28.5	0.25
51	44.5	55.3	0.24
21	15.2	84.5	0.57
0	0	93.4	6.6

[a] Reaction conditions: T = 350 °C, P = 1 atm, W/F = 0.028 h, Time on stream is 0.5 h for each reaction.

peak at 315 °C with increasing intensity and shifted to a higher temperature of 337 °C. According to the results of DRIFTS of pyridine adsorption and NH_3-TPD, this new peak should be related to LAS of Na^+, which adsorbs but is unable to decompose IPA. This assignment is consistent with the decrease of peak at 203 °C, due to exchange of Na^+ with silanols in the internal nests [42].

The quantified acid density from both NH_3-TPD and IPA-TPD are reported in Table 1. Because the overlap between the fragment of $m/z = 41$ from undecomposed IPA and propene at similar temperatures, accurate quantification of the BAS density using propene was not possible. However, as the fragment of $m/z = 16$ from NH_3 was not influenced by the IPA fragment, the NH_3 intensity was used to quantify the density of BAS. On the basis of NH_3 intensity, we measured a BAS density of HZ to be 384 μmol/g, in good agreement with the theoretical value of 406 μmol/g estimated from Si/Al ratio of 40, indicating that most of the strong acid sites are BAS type. Increasing degree of exchange resulted in a decrease in BAS density. A higher acid density from NH_3-TPD than that from IPA-TPD can be attributed to the fact that NH_3

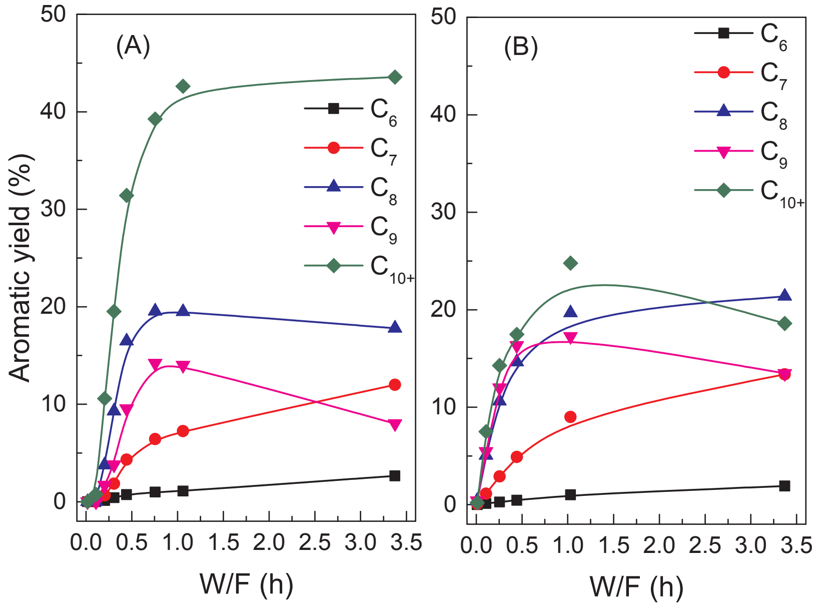

Fig. 7. Aromatic products distribution during (A) propionic acid and (B) 3-pentanone conversion on HZ as a function of W/F. Reaction conditions: T = 350 °C, P = 1 atm, Time on stream is 0.5 h for each W/F.

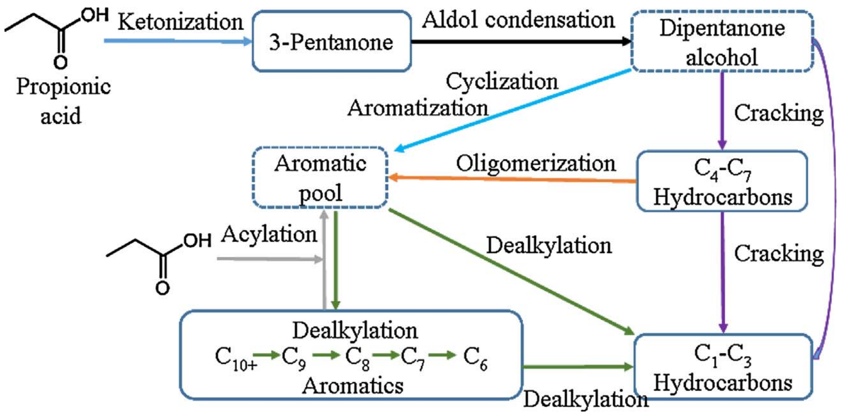

Scheme 1. Proposed major reaction pathway of propionic acid conversion on HZSM-5.

Table 4
Propionic acid conversion on HZ and HNaZ samples with varying density of Brønsted acid sites.[a]

Sample	HZ	HNaZ-1	HNaZ-2	HNaZ-3	HNaZ-4
Conversion (%)	100	77.5	52.9	41.1	23.4
Yield (%)					
3-Pentanone	18.5	39.4	43.7	37.1	22.7
Others	81.5	38.1	9.2	4.0	0.70
Selectivity (%)					
3-Pentanone	18.5	50.8	82.6	90.2	97.0
others	81.5	49.2	17.4	9.8	3.0

[a] Reaction conditions: T = 350 °C, P = 1 atm, W/F = 0.44 h, Time on stream is 0.5 h for each reaction.

Table 5
Comparison of the intrinsic reaction rate and turnover frequency based on Brønsted acid (TOF_{BAS}) of propionic acid and 3-pentanone conversion on HZ and HNaZ samples.[a]

Sample	Propionic acid		3-Pentanone	
	Rate (mmol g_{cat}^{-1} min^{-1})	TOF_{BAS} (min^{-1})	Rate (mmol g_{cat}^{-1} min^{-1})	TOF_{BAS} (min^{-1})
HZ	0.70	1.8	0.50	1.3
HNaZ-1	0.49	1.9	0.26	1.1
HNaZ-2	0.42	2.4	0.10	0.6
HNaZ-3	0.35	3.1	0.04	0.3
HNaZ-4	0.22	5.1	0.0007	0.015

[a] The intrinsic reaction rates were measured at conversion < 10% for both feeds.

adsorbs on both LAS (Na^+ and Al^{3+}) and weak acid sites (Si-OH) in addition to the BAS.

3.2. Conversion of propionic acid and 3-pentanone on HZSM-5

Fig. 6 shows the conversion of propionic acid and evolution of products as a function of space time (W/F) on HZ, with the yield of major products summarized in Table 2. Clearly, 3-pentanone is the only primary product from ketonization of propionic acid at low conversions. The maximum yield of 3-pentanone was achieved at a W/F of 0.2 h. Beyond that, the yield started to decrease with increasing W/F and dropped to zero eventually. In the meantime, the yield of aromatics continuously increased, even after propionic acid being completely converted at a W/F of 0.44 h. The maximum yield of aromatics was about 80%. The aliphatic hydrocarbons of C_1—C_7 appeared to be minor products with total yields < 20%. Table 2 clearly shows that C_{10+} aromatics (particularly for C_{10} of 1,3-dimethyl-4-ethylbenzene) forms prior to C_6—C_9 aromatics at lower W/F. In addition, the yield of 1,3-dimethyl-4-ethylbenzene decreases at high W/F. This result indicates that 3-pentanone may convert to C_{10} aromatics first before cracking/dealkylating to lighter aromatics. This trend becomes more obvious when the yield of aromatics was plotted as a function of W/F. As shown in Fig. 7A, the yields of lighter aromatics, including benzene and

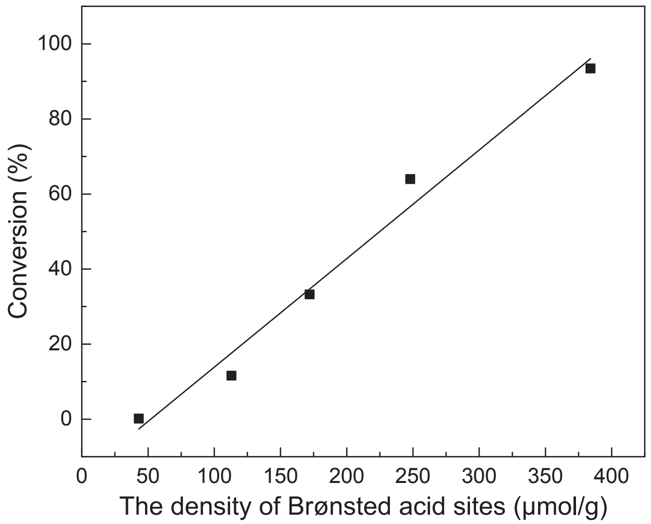

Fig. 9. 3-Pentanone conversion on HZ and HNaZ samples with varying density of Brønsted acid sites. Reaction conditions: T = 350 °C, P = 1 atm, W/F = 0.44 h, Time on stream is 0.5 h for each reaction.

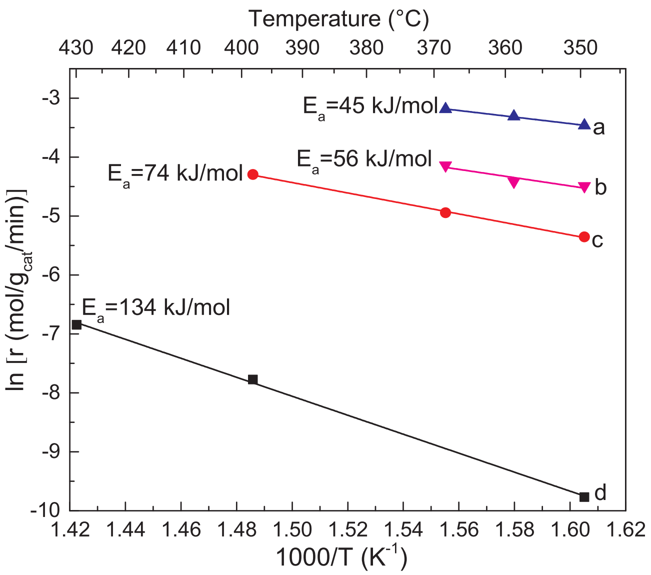

Fig. 10. The Arrhenius plots intrinsic reaction rates of propionic acid (a, b) and 3-pentanone (c, d) conversion and on HZ (a, c) and HNaZ-4 (b, d) samples. The reaction rate was measured at conversion < 15% by varying W/F.

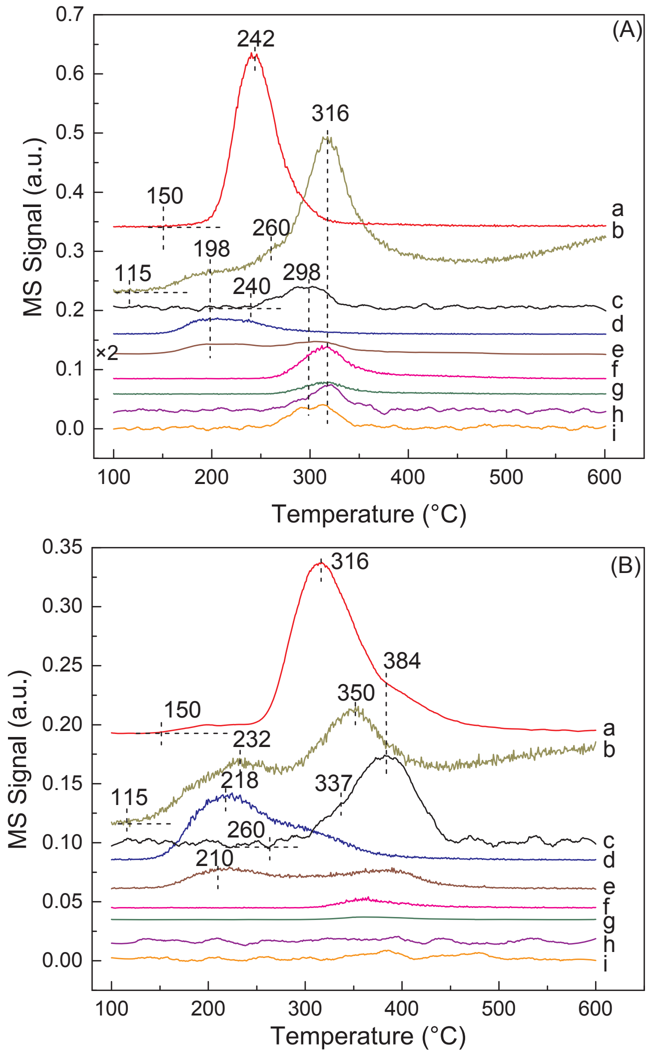

Fig. 11. Temperature programmed desorption profiles of propionic acid on HZ (A) and HNaZ-4 (B). (a) m/z = 44, CO_2; (b) m/z = 18, H_2O; (c) m/z = 86, 3-pentanone; (d) m/z = 74, propionic acid; (e) m/z = 56, methylketene; (f) m/z = 91, C_7 aromatics; (g) m/z = 106, C_8 aromatics; (h) m/z = 120, C_9 aromatics; (i) m/z = 119, C_{10} aromatics. The curve e in figure A is multiplied by a factor of 2.

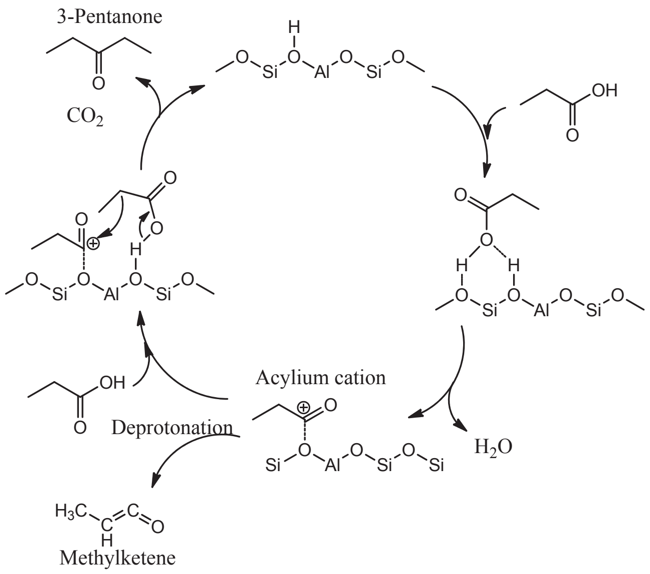

Scheme 2. Proposed surface reaction of ketonization of propionic acid on HZSM-5.

toluene, remain increasing, while the yield of C_8 and C_9 aromatics reaches a maximum and then decreases, indicating the dealkylation of the heavier aromatics.

To further understand the reaction mechanism, 3-pentanone was used as reactant and fed onto HZ. As shown in Fig. 8, complete conversion of 3-pentanone was achieved at a W/F of 1.03 h, indicating that the aldol condensation of 3-pentanone is much less active on HZSM-5 than ketonization of propionic acid. The distribution of overall major products has a similar trend to that of propionic acid feed as reactant but the aromatics yield is about 15% less. In contrast, the yields of aliphatic C_1–C_7 hydrocarbons are higher than those observed from propionic acid feed. In addition, the yield of C_4–C_7 exhibited a maximum at medium W/F. These results suggest that in addition to direct aldol condensation and aromatization of 3-pentanone to aromatics, part of dipentanone alcohol (aldol dimer, which was not observed due to fast dehydration and subsequent reactions) from 3-pentanone may be cracked to C_4–C_7 aliphatic hydrocarbons and then oligomerized to aromatics.

The distributions of major aromatics from propionic acid and 3-pentanone are compared in Fig. 7. The overall trends are similar for the two feeds but the yields of C_{10+} aromatics from propionic acid are ~ 15% higher than that from 3-pentanone. To find the origin of this difference, propionic acid and 3-pentanone were co-fed onto HZ and the results are shown in Table 3. It is evident that at low conversions, the major reaction is ketonization of propionic acid to 3-pentanone, with the absence of cross reaction between propionic acid and 3-pentanone. If ketonization of propionic acid to 3-pentanone and then 3-pentanone conversion to subsequent products are the only reaction pathway, we would expect the same product distributions from the two feeds at high W/F. Obviously, this is not the case. As shown in Scheme 1, besides this major path, a minor path, i.e., acylation of the aromatics with propionic acid followed by further reactions to aromatics, does exist, which would result in higher yields of C_{10+} aromatics.

Indeed, acylation of aromatics with carboxylic acids on zeolites have been explored under mild conditions. For example, Singh et al. investigated the acylation of benzene and toluene with acetic acid over HZSM-5 zeolite in gas phase [43,44]. The maximum yield of acetophenone was achieved at 230 °C, and the yield reduced sharply at higher temperatures due to the consecutive side reactions. These authors suggested that the reaction happens through the acetylium cation (CH_3C^+O) formed from acetic acid attacking the aromatic ring.

3.3. Effect of Brønsted acid site density on the conversion of propionic acid and 3-pentanone

Table 4 compares the conversion of propionic acid and distribution of products on HZ and HNaZ catalysts with varying densities of BAS at the same W/F of 0.44 h. As shown in the table, the conversion of propionic acid decreases as the density of BAS decreases, indicating that BAS is the active site for propionic acid conversion. The selectivity of 3-pentanone increases while the selectivity to other products is reduced with decreasing density of BAS, confirming that 3-pentanone is the primary product, subjecting to further conversion to other products.

The intrinsic reaction rate was measured at a propionic acid conversion < 10%. Turnover frequency (TOF) based on the density of BAS was calculated. As shown in Table 5, the reaction rate decreases with decreasing density of BAS. The TOF reached a constant value of 1.8 min^{-1} for HZ and HNaZ-1 at a density of BAS > 248 μmol/g. The result indicates that BAS is the active site for ketonization of propionic acid on ZSM-5, which is consistent with previous work of acetic acid conversion on ZSM-5 catalyst [21]. However, when the density of BAS was further reduced by Na exchange, the TOF increased to 5.1 min^{-1} on HNaZ-4.

Fig. 9 shows the conversion of 3-pentanone on different catalyst samples with varying BAS densities at the same W/F of 0.44 h. The conversion of 3-pentanone increases linearly with the increasing BAS

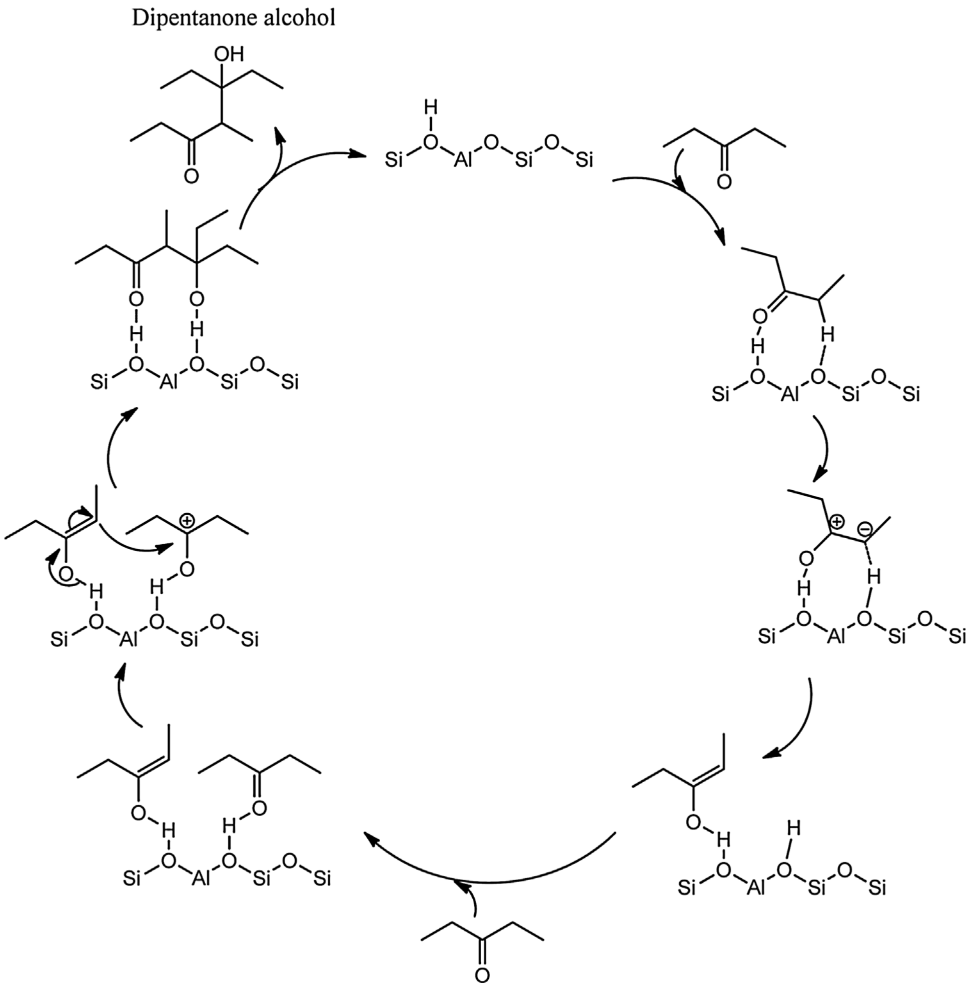

Scheme 3. Proposed surface reaction of aldol condensation of 3-pentanone on HZSM-5.

density, indicating that BAS is also the active site for aldol condensation of 3-pentanone on ZSM-5 and consistent with the previous result of acetone conversion on zeolites [45]. The intrinsic reaction rate and TOF of 3-pentanone at conversion < 10% was also summarized in Table 5. The data in Table 5 shows that the reaction rate of 3-pentanone is lower than that of propionic acid. Similar to the conversion of propionic acid, TOF is almost constant for HZ and HNaZ-1 at a BAS density > 248 μmol/g, confirming the active site for aldol condensation is BAS. However, TOF decreases significantly when the BAS density decreases further.

The Arrhenius plots of propionic acid and 3-pentanone conversion on HZ and HNaZ-4 are compared in Fig. 10. The activation energy of aldol condensation on HZ is about 30 kJ/mol higher than that of ketonization. On Na-exchanged HNaZ-4, activation energies for both reactions are increased with respect to those on HZ.

3.4. Temperature programmed desorption of propionic acid on HZSM-5 and HNaZSM-5

To understand the reaction mechanism on ZSM-5, TPD of propionic acid on HZ and HNaZ-4 were carried out and the results are shown in Fig. 11. The TPD profiles from the two samples are significantly different. On HZ, the formation of H_2O (m/z = 18) started at 115 °C precedes CO_2 (m/z = 44) formation centered at 242 °C and 3-pentanone (m/z = 86) formation centered at 298 °C (Fig. 11A). As shown in Scheme 2, the result indicates that the reaction starts with formation of acyl species ($CH_3CH_2C^*O$) on BAS through dehydration (protonation of $-OH$ of the propionic acid by BAS followed by elimination of H_2O), consistent with the previous reports of acetic acid conversion [16,20,21]. It is interesting to note that the first H_2O peak at 198 °C is coincided with a weak peak of methylketene (CH_3CHCO, m/z = 74), which indicates the deprotonation of acylium cation ($CH_3CH_2C^+O$) and regeneration of BAS. The third H_2O formation peak at 316 °C is later than 3-pentanone but coincided with the formation of $C_7{-}C_{10}$ aromatics, which indicates that this peak is associated with 3-pentanone conversion to aromatics. It should be noted that the C_{10} aromatics formation is slightly earlier than other aromatics.

Compared to HZ, the HNaZ-4 sample with the least amount of BAS produced more methylketene and 3-pentanone, while the formation temperatures of CO_2, H_2O (2nd peak) and 3-pentanone were shifted to higher values (Fig. 11B). In addition, almost no aromatics were observed. These results indicate that the formation of acyl species occurs on BAS and fewer BAS limited the consecutive reactions of acyl species and resulted in methylketene through deprotonation and desorption. The reduction of the consecutive reactions from 3-pentanone due to fewer BAS also resulted in more 3-pentanone in the products from the propionic acid. It is important to note that the major 3-pentanone peak is accompanied by a CO_2 shoulder peak at 384 °C.

3.5. Reaction mechanism of propionic acid on HZSM-5 and HNaZSM-5

On the basis of the above experimental results, a mechanism of ketonization of propionic acid can be proposed (Scheme 2). Propionic acid adsorbs on BAS of zeolite through protonation of its hydroxyl O with hydroxyl H atom being adsorbed on adjacent framework O atom, which can undergo a dehydration (dehydroxylation of propionic acid with proton of BAS forming H_2O) to the acyl species ($CH_3CH_2C^*O$) in equilibrium with the acylium cation ($CH_3CH_2C^+O$). Even though the

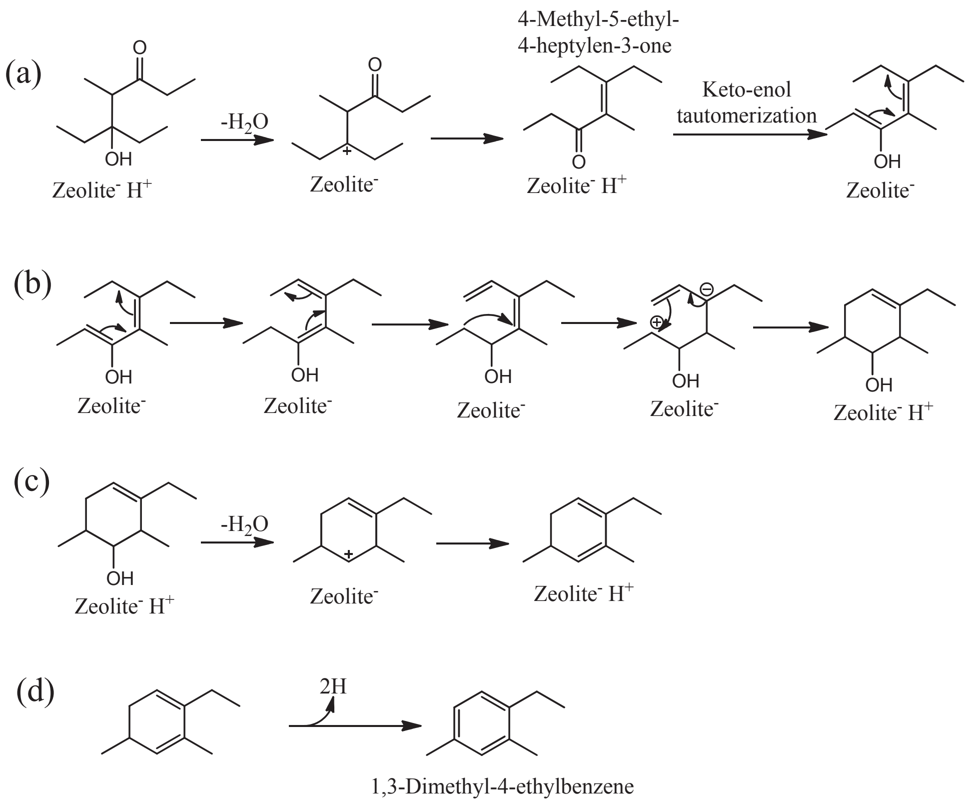

Scheme 4. Proposed surface reaction of dipentanone alcohol undergoes through (a) Dehydration, (b) Ring-closure, (c) Dehydration, and (d) Hydride transfer to C_{10} aromatic of 1,3-dimethyl-4-ethylbenzene on HZSM-5.

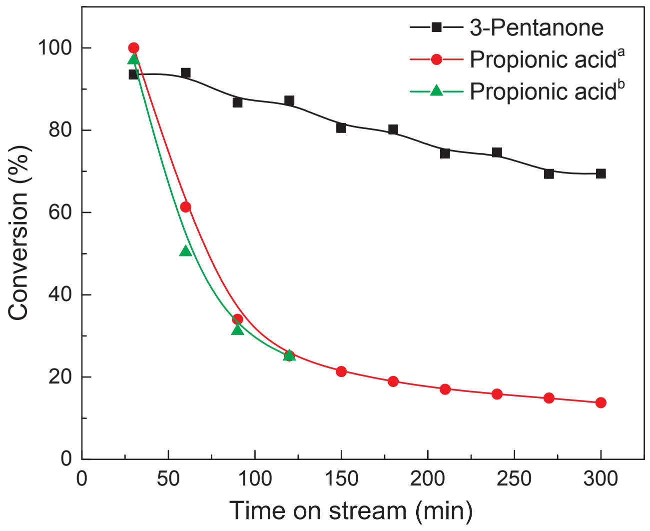

Fig. 12. Effect of time on stream on the conversion of propionic acid and 3-pentanone on HZ. [a]Propionic acid reaction on fresh HZ. [b]Propionic acid reaction on regenerated HZ. Reaction conditions: W/F = 0.44 h; T = 350 °C; P = 1 atm.

adsorption through the hydroxyl oxygen is about 10 kJ/mol weaker than the adsorption through carbonyl oxygen [46], the former configuration is more susceptible for dehydration than the latter one. A second propionic acid molecule adsorbs on the vicinal framework O through the H atom of hydroxyl could transfer this H atom as a proton to the basic framework O [17]. The resulting intermediate became nucleophilic and could attack the acylium cation [16,20] and eliminate CO_2 to produce 3-pentanone. The acylium cation ($CH_3CH_2C^+O$) may also desorb as methylketene (CH_3CHCO) through deprotonation without participating further reaction.

Scheme 3 shows the possible surface reactions for the aldol condensation of 3-pentanone. 3-Pentanone adsorbs on BAS via protonation, which induces a partial charge transfer from the framework to the carbonyl group and abstracts the α-H on adjacent framework O, resulting in formation of the enol. This is similar to the enol formation from acetone on HZSM-5 [23,47]. Another 3-pentanone molecule adsorbs on the newly formed BAS. The activated carbonyl carbon can easily react with the unstable C═C of enol [48] to form dipentanone alcohol. While the dipentanone alcohol is the primary product of aldol condensation, it was not observed in the products. This result shows that the dipentanone alcohol is consumed quickly in dehydration and the subsequent reactions, consistent with the previous study by Biaglow et al. [48]. As shown in Scheme 4, the dipentanone alcohol may undergo dehydration, ring closure, dehydration, and hydride transfer to C_{10} aromatics of 1,3-dimethyl-4-ethylbenzene, as has been observed in the products (Table 2). As shown in Scheme 1, the C_{10} aromatics may dealkylate to C_6–C_9 aromatics as well as C_1–C_2 hydrocarbons. In addition, acylation of aromatics followed by consecutive reactions may form C_{10+} aromatics, such as methylated naphthalenes, as has been observed experimentally (Table 2). Formation of C_{10+} aromatics through tripentanone alcohol is not expected due to pore size limitations (i.e., transition state or product shape selectivity). The dipentanone alcohol may also crack to C_4–C_7 hydrocarbons and then cyclize and aromatize to aromatics. One possible pathway for C_3 formation is dehydration, followed by hydride transfer and dehydration, similar to that was proposed for propanal [49].

The results clearly established that the active sites for both ketonization and aldol condensation are BAS. However, the TOFs of the two reactions show very different dependences on the BAS density (Table 5). The TOF for aldol condensation decreases as the BAS density is reduced. As shown in Scheme 3, bimolecular aldol condensation requires two adjacent BASs. Furthermore, the formation of enol requires abstraction of α-H by the adjacent framework O. Decreasing BAS density by Na exchange increases probability of Na^+ in presence next to BAS and reduces the activity toward α-H abstraction and formation of enol, and eventually resulted in the reduced turnover of the aldol condensation and significantly increased the apparent activation energy

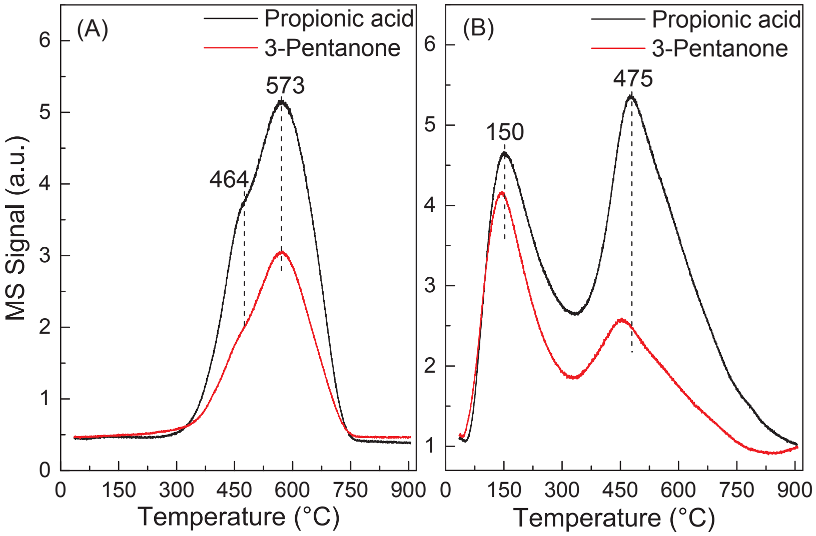

Fig. 13. Temperature programmed oxidation profiles of spent catalysts after 5 h on stream: (A) CO_2 and (B) H_2O. Reaction conditions are shown Fig. 12.

(Fig. 10). Another possible reason is related to the reduction of acid strength of BAS as a function of Na exchange, as shown by the shift of high temperature peak to lower values in NH_3-TPD (Fig. 4) and propene peak shift to higher temperatures in IPA-TPD (Fig. 5B). When the acid strength of BAS is lower than a critical value, the BAS sites may not be able to activate and catalyze the aldol condensation of 3-pentanone at low temperature of 350 °C, resulting in an almost zero conversion in Fig. 9. Similar observation has been reported for o-xylene isomerization and toluene alkylation with methanol on ZSM-5 catalysts with different degree of Na exchange [50].

However, the TOF for ketonization increases with decreasing BAS density due to Na exchange (Table 5). Two factors may contribute to this observation. First, ion exchange between proton of propionic acid and Na^+ in HNaZ samples results in formations of BAS and sodium propionate. Indeed, Xu et al. showed the IR evidence of BAS formation in-situ by exposing NaY to propionic acid in the temperature range of 150–300 °C [51]. Apparently, these BASs formed in-situ catalyze additional ketonization. However, this type of in-situ ion exchange is not available between Na^+ and 3-pentanone. Second, two sodium propionates could decompose to 3-pentanone, CO_2 and Na_2O [52]. And Na_2O can then react with the proton of BAS formed in-situ [52]. The decomposition of bulk sodium propionate has been reported to happen at temperatures > 350 °C [53]. Therefore, we assign the 3-pentanone peak of low temperature shoulder at 337 °C to BAS catalyzed ketonization, while the peak at 384 °C to the decomposition of sodium propionate, resulting in CO_2 formation at the same temperature (Fig. 11B). Both factors contribute to the improved TOF at low BAS density due to Na exchange. Evidently, the newly formed BAS and decomposition of propionate are less active for the ketonization reaction (Fig. 11), resulting in reduced mass based intrinsic reaction rate (Table 5) and increased the activation energy (Fig. 10).

3.6. Deactivation

Fig. 12 compares the conversion of propionic acid and 3-pentanone on HZ as function of time on stream at the same W/F of 0.44 h. Both feeds showed a similar initial conversion. A sharp deactivation in the propionic acid feed is observed at ~100 min, and then the rate of deactivation decreases. In contrast, the 3-pentanone feed causes a slow deactivation. TPO was carried out to estimate the coke deposited on the catalyst after 300 min. Both CO_2 and CO were produced during TPO, and CO was lumped as equal moles of CO_2 based on the calibration, as shown in Fig. 13. The quantified coke formation for propionic acid and 3-pentanone are 5.0% and 2.5%, respectively. Interestingly, the ratio of the peak areas of CO_2 (Fig. 13A) to H_2O at high temperature of 475 °C (Fig. 13B, the low temperature peak at 150 °C is associated with desorption of physisorbed H_2O) are 0.92 and 1.14 for propionic acid and 3-pentanone feeds, respectively. This result indicates that the coke formed is more hydrogen deficient in a 3-pentanone feed than a propionic acid feed.

The deactivation profile and TPO could help to understand the mechanism of catalyst deactivation during propionic acid conversion. Calculations showed that the adsorption energy of propionic acid on HZSM-5 varies from −116 to −143 kJ/mol, depending on the adsorption configuration [46]. On the other hand, the adsorption energy of acetone on HZSM-5 was measured to be only −61 kJ/mol [54]. The adsorption energy of 3-pentanone is expected to be higher than that of acetone due to increased van der Waals interactions as a result of increased molecular size but should be smaller than that of propionic acid. This strong adsorption of propionic acid on the catalytic sites would result in fast deactivation at the initial stage of reaction and produces relatively H rich coke. In contrast, 3-pentanone adsorbs relatively weaker and the main deactivation mechanism may originate from the products, such as aromatics as the sources of relatively H-deficient coke. In addition, the C_{10+} aromatics produced from propionic acid may block the channel of zeolite, thereby, contributing to a faster deactivation.

The used HZ sample was regenerated by calcination at 550 °C for 4 h. The XRD pattern (data not shown) of the regenerated sample showed the MFI structure is well-preserved. The regenerated HZ sample was tested for propionic acid conversion. As shown in Fig. 12, it showed a similar conversion profile as a function of time on stream to that of the fresh HZ sample. The results indicate that the major reason for zeolite deactivation is coke formation, and the zeolite can be regenerated by calcination.

4. Conclusion

A comparative study of propionic acid and 3-pentanone conversion on the ion-exchanged HZSM-5 zeolite at 350 °C was investigated. The results show that the primary reaction of propionic acid is ketonization to 3-pentanone, and the secondary reaction is the sequential aldol condensation for dipentanone alcohol formation. The dipentanone alcohol undergoes dehydration, cyclization, dehydration and hydride transfer rapidly, resulting in C_{10} aromatics, which could then be dealkylated to lighter aromatics. It can also be cracked to produce C_4—C_7 hydrocarbons, followed by cyclization and oligomerization to aromatics. Acylation of the aromatics with propionic acid also contributes to C_{10+} aromatics formation, although minor contribution, resulting in a higher C_{10+} aromatics yield with the propionic acid feed than that with the 3-pentanone feed. Temperature programmed desorption of propionic acid indicates that the reaction initiates with acylium cation formation on the Brønsted acid sites through dehydration. Comparison of turnover frequency of the reactions on HNaZSM-5 indicates that Brønsted acid sites are the active site for both ketonization and aldol condensation reactions. The propionic acid feed deactivates the catalyst faster than the 3-pentanone feed due to the stronger adsorption of propionic acid on the acid sites of ZSM-5.

Acknowledgments

The authors thank the support from National Natural Science Foundation of China (21676194 and 21373148) and Ministry of Education of China for Program of New Century Excellent Talents in University (NCET-12-0407).

References

[1] M. Besson, P. Gallezot, C. Pinel, Chem. Rev. 114 (2014) 1827–1870.
[2] M.J. Climent, A. Corma, S. Iborra, Green Chem. 16 (2014) 516–547.
[3] A. Oasmaa, D.C. Elliott, J. Korhonen, Energy Fuels 24 (2010) 6548–6554.
[4] A.V. Bridgwater, Biomass Bioenergy 38 (2012) 68–94.
[5] T.N. Pham, D. Shi, D.E. Resasco, J. Catal. 314 (2014) 149–158.
[6] M. Gliński, J. Kijeński, A. Jakubowski, Appl. Catal. A 128 (1995) 209–217.
[7] R.W. Snell, B.H. Shanks, Appl. Catal. A 451 (2014) 86–93.
[8] S. Muller, Y. Liu, F.M. Kirchberger, M. Tonigold, M. Sanchez-Sanchez, J.A. Lercher, J. Am. Chem. Soc. 138 (2016) 15994–16003.
[9] W.O. Haag, R.M. Lago, P.G. Rodewald, J. Mol. Catal. 17 (1982) 161–169.
[10] X. Zhu, L.L. Lobban, R.G. Mallinson, D.E. Resasco, J. Catal. 271 (2010) 88–98.
[11] T.Q. Hoang, X. Zhu, T. Sooknoi, D.E. Resasco, R.G. Mallinson, J. Catal. 271 (2010) 201–208.
[12] X. Zhu, R.G. Mallinson, D.E. Resasco, Appl. Catal. A 379 (2010) 172–181.
[13] T.Q. Hoang, X. Zhu, T. Danuthai, L.L. Lobban, D.E. Resasco, R.G. Mallinson, Energy Fuels 24 (2010) 3804–3809.
[14] J. Wang, Z. Zhong, K. Ding, Z. Xue, Bioresour. Technol. 212 (2016) 6–10.
[15] A.G. Gayubo, A.T. Aguayo, A. Atutxa, R. Aguado, M. Olazar, J. Bilbao, Ind. Eng. Chem. Res. 43 (2004) 2619–2626.
[16] C.D. Chang, A.J. Silvestri, J. Catal. 47 (1977) 249–259.
[17] J.A. Martens, M. Wydoodt, P. Espeel, P.A. Jacobs, Stud. Surf. Sci. Catal. 78 (1993) 527–534.
[18] D.E. Resasco, B. Wang, S. Crossley, Catal. Sci. Technol. 6 (2016) 2543–2559.
[19] A. Witsuthammakul, T. Sooknoi, Catal. Sci. Technol. 6 (2016) 1737–1745.
[20] G.J. Hutchings, P. Johnston, D.F. Lee, A. Warwick, C.D. Williams, M. Wilkinson, J. Catal. 147 (1994) 177–185.
[21] A. Gumidyala, T. Sooknoi, S. Crossley, J. Catal. 340 (2016) 76–84.
[22] O. Kikhtyanin, R. Bulánek, K. Frolich, J. Čejka, D. Kubička, J. Mol. Catal. A: Chem. 424 (2016) 358–368.
[23] J. Limtrakul, B. Boekfa, P. Pantu, M. Probst, J. Phys. Chem. C 114 (2010) 15061–15067.
[24] Q. Sun, G. Chen, H. Wang, X. Liu, J. Han, Q. Ge, X. Zhu, ChemCatChem 8 (2016) 551–561.
[25] P. Sazama, B. Wichterlova, J. Dedecek, Z. Tvaruzkova, Z. Musilova, L. Palumbo, S. Sklenak, O. Gonsiorova, Micropor. Mesopor. Mat. 143 (2011) 87–96.
[26] S. Kotrel, J.H. Lunsford, H. Knözinger, J. Phys. Chem. B 105 (2001) 3917–3921.
[27] C. J. Chem. Soc. OteroáAreÓn, Faraday Trans. 88 (1992) 2959–2969.
[28] M.B. Sayed, R.A. Kydd, R.P. Cooney, J. Catal. 88 (1984) 137–149.
[29] M. Huang, S. J. Chem. Soc. Kaliaguine, Faraday Trans. 88 (1992) 751–758.
[30] A. Jia, L. Lou, C. Zhang, Y. Zhang, S. Liu, J. Mol. Catal. A: Chem. 306 (2009) 123–129.
[31] V. Vishwanathan, K.W. Jun, J.W. Kim, H.S. Roh, Appl. Catal. A 276 (2004) 251–255.
[32] T. Inui, H. Nagata, F. Okazumi, H. Matsuda, Catal. Lett. 13 (1992) 297–304.
[33] Y. Xu, W. Liu, S.T. Wong, L. Wang, X. Guo, Catal. Lett. 40 (1996) 207–214.
[34] Y. Ono, Y. Fujii, H. Wakita, K. Kimura, T. Inui, Appl. Catal. B: Environ. 16 (1998) 227–233.
[35] K.Y. Lee, M.Y. Kang, S.K. Ihm, J. Phys. Chem. Solids 73 (2012) 1542–1545.
[36] D. Mao, W. Yang, J. Xia, B. Zhang, Q. Song, Q. Chen, J. Catal. 230 (2005) 140–149.
[37] H. Sato, Catal. Rev. 39 (1997) 395–424.
[38] J. Valyon, G. Onyestyák, L.V. Rees, J. Phys. Chem. B 102 (1998) 8994–9001.
[39] C. Pereira, R.J. Gorte, Appl. Catal. A 90 (1992) 145–157.
[40] J.G. Tittensor, R.J. Gorte, D.M. Chapman, J. Catal. 138 (1992) 714–720.
[41] A.I. Biaglow, D.J. Parrillo, R.J. Gorte, J. Catal. 144 (1993) 193–201.
[42] D.J. Parrillo, D. Dolenec, R.J. Gorte, R.W. Mccabe, J. Catal. 142 (1993) 708–718.
[43] A.P. Singh, A.K. Pandey, J. Mol. Catal. A: Chem. 123 (1997) 141–147.
[44] A.K. Pandey, A.P. Singh, Catal. lett. 44 (1997) 129–133.
[45] S. Herrmann, E. Iglesia, J. Catal. 346 (2017) 134–153.
[46] X. Li, Y. Zhao, S. Wang, Y. Zhu, G. Yang, Catal. Lett. 146 (2016) 2015–2024.
[47] M. Xu, W. Wang, M. Hunger, Chem. Commun. (2003) 722–723.
[48] A.I. Biaglow, J. Sepa, R.J. Gorte, D. White, J. Catal. 151 (1995) 373–384.
[49] F. Lin, Y.H. Chin, J. Catal. 311 (2014) 244–256.
[50] J. Datka, Z. Piwowarska, J. Rakoczy, B. Sulikowski, Zeolites 8 (1988) 199–204.
[51] B. Murphy, M.E. Davis, B. Xu, Top. Catal. 58 (2015) 393–404.
[52] L.M. Parker, D.M. Bibby, I.J. Miller, J. Catal. 129 (1991) 438–446.
[53] J.J. Duruz, H.J. Michels, A.R. Ubbelohde, J. Chem. Soc. B: Phys. Org. (1971) 1505–1509.
[54] A. Rattanasumrit, V. Ruangpornvisuti, J. Mol. Catal. A: Chem. 239 (2005) 68–75.